This article has been accepted for inclusion in a future issue of this journal. Content is final as presented, with the exception of pagination.

Coverage Optimization for Reliable UAV-Assisted 5G/6G Communication Systems

Bilel Ben Saoud, *Student Member, IEEE*, and Leïla Nasraoui, *Senior Member, IEEE*

***Abstract*—Unmanned aerial vehicles (UAVs) play a pivotal role in 5G/6G wireless communication systems due to their deployment flexibility. This article explores optimal UAV positioning to maximize coverage in hybrid aerial–ground communication links. Exploiting a probabilistic line-of-sight (LOS) model, we examine coverage radius behavior in mixed urban and suburban environments to meet specific quality-of-service (QoS) targets. The analysis reveals that the coverage radius expands as the probability of LOS increases, which in turn increases with the UAV height. However, beyond a certain height, path loss becomes dominant, and further increases in altitude negatively impact the coverage radius. By studying the maximum coverage radius for minimum signal strength and spectral efficiency requirements, we numerically determine a configuration space of UAV altitudes and the corresponding maximum radius that satisfies the target QoS. The results illustrate a dual-regime behavior, where coverage increases with altitude up to a certain value, beyond which it declines, indicating the existence of an optimal altitude for reliability. In addition, the analysis of ground surface effects shows that flying over concrete surfaces significantly enhances coverage, offering a radius up to five times larger compared to rough, vegetated surfaces.**

***Index Terms*—5G/6G, air–ground link, coverage, line-of-sight (LOS) probability, network reliability, unmanned aerial vehicle (UAV).**

NOMENCLATURE

Symbol	Signification
h_1	UAV altitude.
h_2	G-UE altitude.
ξ	SNR threshold.
C	Spectral efficiency.
C_0	Spectral efficiency threshold.
$h_{\min}$	Minimum height of the buildings.
$h_{\max}$	Maximum height of the buildings.
ϕ	Elevation angle.
λ	Poisson process rate of building θ.
r	Horizontal distance.
l	Slant distance.
O	UAV projection onto the ground.
R	Coverage radius.
P_t	Transmission power.
σ_n^2	Noise power.
α	Pathloss exponent.
Λ	Signal wavelength
Ω	Channel power loss/gain factor.
$\bar{\Omega}$	Mean value of Ω.
K	Rice factor.
$f_{\Omega_{\text{Ri}}}$/ $f_{\Omega_{\text{Ra}}}$	PDF of Ω in Rice/Rayleigh channel.
PD/PC	Probability of detection/connectivity.
PD_{Ri}/PD_{Ra}	PD for Rice/Rayleigh channel.
PC_{Ri}/PC_{Ra}	PC for Rice/Rayleigh channel.
P_{LOS}	Probability of line of sight.
P_{NLOS}	Probability of non line of sight.
$g_{C_{\text{Ri}}}(c)$/ $g_{C_{\text{Ra}}}(c)$	PDF of the SE for Rice/Rayleigh channel.
$\text{PD}_{\text{target}}$	Target probability of detection.
$\text{PC}_{\text{target}}$	Target probability of connectivity.
(h_1, R_{h_1})	Set of configuration space.
$(h_{1,\text{opt}}, R_{\text{h}_1,\text{opt}})$	Optimal configuration.
ϕ_{opt}	Optimal elevation angle.
ρ	Power from scattered components.
β_0	Soil roughness.
κ_0 and $\kappa_{\frac{\pi}{2}}$	Parameters of concrete surfaces.

I. INTRODUCTION

The 5G and beyond 5G systems have expanded mobile communications beyond the human-centric market to include the Internet of Things (IoT) and industrial applications, supporting three key usage scenarios: enhanced mobile broadband [1], ultrareliable low-latency communications [2], [3], and massive machine-type communication, including device-to-device connectivity [4], [5]. These systems enable innovative services, such as mobile data collection [6], [7], proximity-based services [8], [9], connected and automated mobility [10], virtualization [11], user tracking and discovery [12], [13], and artificial intelligence-powered secured crowd-sourcing [14], [15], among others. Also, unmanned aerial vehicles (UAVs) and unmanned aircraft systems (UAS) became standard technologies in the 5G system and are expected to play a significant role in the 6G system [16], [17]. Their deployment ensures robust and reliable connectivity, supporting a wide range of critical application scenarios. These include addressing network congestion during large-scale events such as sports tournaments, concerts, and festivals; providing emergency communication infrastructure following natural disasters such as earthquakes, hurricanes, or floods where terrestrial networks are often compromised;

Received 9 January 2024; revised 15 June 2024, 24 September 2024, and 12 December 2024; accepted 12 January 2025. This work was supported by the Ministry of Higher Education and Scientific Research of Tunisia under Project PEJC2024-D6P11. *(Corresponding author: Leïla Nasraoui.)*

The authors are with the COSIM Research Lab., Higher School of Communications (SUP'COM), University of Carthage, Carthage 1054, Tunisia, and also with the National School of Computer Sciences (ENSI), University of Manouba, La Manouba 2010, Tunisia (e-mail: bilel.bensaoud@ensi-uma.tn; leila.nasraoui@supcom.tn).

Digital Object Identifier 10.1109/JSYST.2025.3532232

1937-9234 © 2025 IEEE. All rights reserved, including rights for text and data mining, and training of artificial intelligence and similar technologies. Personal use is permitted, but republication/redistribution requires IEEE permission. See https://www.ieee.org/publications/rights/index.html for more information.

Authorized licensed use limited to: University of the West of England. Downloaded on March 02,2025 at 08:56:53 UTC from IEEE Xplore. Restrictions apply.

This article has been accepted for inclusion in a future issue of this journal. Content is final as presented, with the exception of pagination.

and enabling temporary network deployment in remote areas requiring short-term connectivity, such as construction sites or archaeological expeditions. However, large variations in target locations, severe tree and shadow occlusions, and complex urban environments present significant challenges for coverage and signal reception. The positioning of both ground nodes and UAVs is critical, as it directly influences coverage performance, connection reliability, and service availability. Optimal placement is then a key factor in the design of effective aerial-to-ground (A2G) links.

While some studies have focused on optimizing ground node positioning for maximum coverage using UAV-acquired data, such as multispectral images [19], or through the placement of anchor nodes to assist in locating equipment [20], [21], [22], other research has developed methods to determine the optimal UAV position to enhance coverage [23], [24], [26]. Indeed, by operating above ground level, UAVs have the flexibility to position themselves for unobstructed line-of-sight (LOS) links to ground nodes, enabling new advancements in IoT applications. This capability, combined with the massive connectivity offered by UAV-enabled 5G/6G networks, is driving innovation in the field.

A. Related Works

Azari et al. [23] investigated optimal UAV positioning for A2G communication through the Rician channel, considering both LOS and non LOS (NLOS) components. The study identified an optimal UAV height that maximizes coverage for a ground node with an exponential Rician K-factor, based on outage probability. Similarly, Nasraoui and Roy [24] optimized UAV relay node positioning to enhance network connectivity using a physics-based Rice channel and showed a unique optimal height for maximum deployment area, based on signal strength and Shannon capacity. In [25], the proposed algorithm aimed to determine a suboptimal set of UAV positions from predefined locations by creating a combination matrix and deriving the signal-to-interference-plus-noise ratio (SINR) for all positions. Then, it retains the subset of deployment locations satisfying the SINR, the UAV limited hovering altitude, and the restricted operating zone.

Later, in [26], a reinforcement learning method using a multiagent collaborative environment was proposed, where each UAV acts as an independent agent that trains its local model with deep-Q-network and determine its strategy. Federated learning allows UAVs to periodically upload gradients and weights to a server for aggregation and receive updated model parameters for the next training round, improving network coverage. In [27], a system using UAVs in mountainous areas was developed exploiting a geometry-based NLOS probability model for reliability analysis. While effective, the predicted reliability occasionally fails to meet the requirements. To minimize the sum of UAV flight distance, a solution for joint positioning and trajectory planning was proposed in [28]. The model selects optimal UAV locations from candidate points generated using a fuzzy candidate points selection algorithm, formulated as a capacitated P-median problem and solved iteratively. The approach ensured required coverage for terrestrial users and solved the optimization efficiently.

Existing works highlight the importance of UAV positioning on network performance. The authors in [23], [24], and [25] show that the maximum coverage area depends on the signal-to-noise ratio (SNR) or the transmission power and identify an optimal altitude for coverage. However, they assume a permanent LOS component, which is unrealistic in urban environment. Learning-based methods [26] improved network utility and coverage but suffer from communication delays due to the huge overhead carrying information interaction. Also, limited transmission power, energy, and dynamic environments make decision making for multiple UAVs challenging. Another drawback in some approaches is to reduce complexity by approximation to a simple model for feasibility [25] or limiting position candidates [28], which leads to suboptimal solutions.

B. Contributions

In this article, we thoroughly analyze coverage behavior in UAV-assisted wireless networks to ensure reliable connection for ground users. We particularly examine environmental impacts on coverage, focusing on worst-case edge coverage and average spectral efficiency (ASE) for randomly positioned users to meet desired quality-of-service (QoS). The main contributions of this article are follows.

1) Usage of a hybrid model combining both LOS and NLOS scenarios arising respecting a probabilistic Poisson distribution to capture the varying environmental characteristics of suburban and urban areas, which influence the LOS probability. For the LOS link, we apply the Rice distribution, utilizing two distinct models for the K-factor, while the Rayleigh distribution is used for the NLOS case.
2) Deriving the probability of detection (PD), defined as the likelihood of achieving a fixed SNR level, and the probability of connectivity (PC), which represents the probability of ensuring a fixed ASE within the coverage area. The resulting expressions highlight the relationships between maximum coverage area, ground conditions, SNR thresholds, UAV altitude, and the LOS probability.
3) Analysis of the impact of buildings' density and characteristics in urban and suburban areas, the LOS probability, and the effects of soil composition for concrete and vegetated terrain with varying levels of roughness
4) Performing a numerical optimization of the UAV's position to maximize coverage while ensuring a target QoS with PD and PC greater than 0.9. The results are then compared across the two aforementioned K-factor models in both urban and suburban environments.

The rest of this article is organized as follows. Section II presents the system model and describes the LOS probability, the SNR, and the fading models. Altitude-dependent coverage and spectral efficiency (SE) are studied in Sections III and IV highlighting the impact of the altitude on the network performance. In Section V, the K-factor models are examined for two different surface types. A thorough investigation of altitude optimization

Authorized licensed use limited to: University of the West of England. Downloaded on March 02,2025 at 08:56:53 UTC from IEEE Xplore. Restrictions apply.

This article has been accepted for inclusion in a future issue of this journal. Content is final as presented, with the exception of pagination.

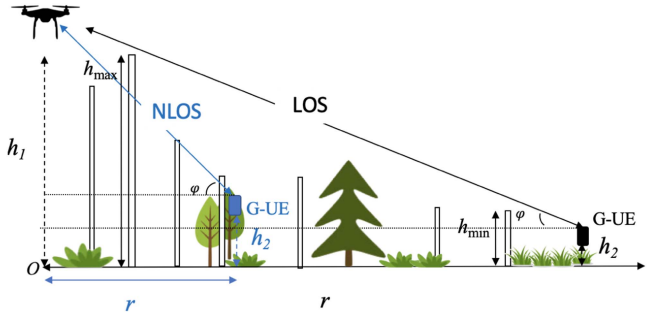

Fig. 1. Example of a typical A2G communication environment compromising LOS and NLOS channels with a 1-D building model.

is presented in Section VI with analysis and discussion. Finally, Section VII concludes this article.

II. System Model

We consider an A2G communication channel where a UAV serves as a relay for existing ground devices, forming a UAV-assisted wireless network. The UAV operates in both urban and suburban environments, as depicted in Fig. 1. Specifically, the system consists of a relay UAV positioned at an altitude h_1, facilitating connections to ground user equipments (G-UEs) that communicate via the 5G network [29]. The G-UEs are located at an altitude h_2, with a horizontal distance r from the projection of the UAV onto the ground plane at point O, and an elevation angle of ϕ. The modeled environment includes a mix of urban and suburban areas, characterized by a substantial presence of buildings, which create an LOS and NLOS dichotomy. These buildings are represented as vertical 1-D objects randomly distributed along the radial axis between the UAV and the G-UE. For reference, the symbols used throughout this analysis are summarized in the Nomenclature.

Depending on its location, each G-UE falls into one of two primary propagation categories: receivers that experience an LOS or near-LOS condition, modeled using a Rician channel, or receivers that operate under NLOS conditions but still receive coverage through strong reflections and diffractions, modeled by a Rayleigh channel. The classification into these two groups is determined by a combination of LOS and NLOS models, which is averaged using a probability of LOS. This probability is estimated through the Poisson spatial point process for building locations, as detailed in Section II-A.

A. LOS Probability Model

The two dominant propagation groups, corresponding to the LOS and NLOS conditions, are mathematically linked as follows:

$$P_{\text{NLOS}} = 1 - P_{\text{LOS}}. \tag{1}$$

Methods for determining the probability of a geometrical LOS between a ground node and an aerial one take into account critical terrain and environmental features. They are often based on statistical models derived from empirical data, such as the spatial channel and the WINNER II models [30]. In this study, we employ an analytical model to estimate LOS probability using the Poisson spatial point process for building locations [31]. This approach introduces a novel model for estimating LOS/NLOS propagation in urban and suburban environments. The model uses a 1-D Poisson process to represent building placements, which aligns with observed distributions of average building density and height. The LOS probability depends on the elevation of both endpoints and the aggregate clutter loss caused by obstructions from buildings or natural elements.

The scenario geometry is illustrated in Fig. 1, where h_{max} and h_{min} represent the maximum and minimum building heights, respectively, in the area under study. Buildings are randomly distributed along the radial axis connecting the G-UE to the UAV, modeled as a spatially varying Poisson process with a local rate $\lambda(r)$ per unit length. For shorter distances, this rate can be approximated by a local average λ. The building heights follow a probability density function (PDF) with finite support, characterized by a unimodal shape that increases monotonically to a peak, and then, decreases (e.g., uniform and Beta PDFs).

Under the assumption of a Poisson arrival process for buildings with a rate of λ, and using the generalized Beta distribution to model building height, the probability of LOS, $P_{\text{LOS}}(r)$, at a distance r is expressed as follows [31]:

$$P_{\text{LOS}}(r) = \exp\left(-\frac{\lambda r}{\Delta \text{H}} \frac{\tilde{h}_{\text{min}} + \tilde{h}_{\text{max}}}{2}\right) \tag{2}$$

where $\Delta H = h_1 - h_2$ is the cut-off height for LOS, $\tilde{\text{h}}_{\text{min}} = h_{\text{min}} - h_2$, and $\tilde{\text{h}}_{\text{max}} = h_{\text{max}} - h_1$. Given that $\Delta H = \tan(\phi) r$, the probability P_{LOS} can be rewritten as a function of the elevation angle ϕ as

$$P_{\text{LOS}}(r) = \exp\left(-\frac{\lambda}{\tan(\phi)} \frac{\tilde{h}_{\text{min}} + \tilde{h}_{\text{max}}}{2}\right). \tag{3}$$

B. SNR Model

As shown in Fig. 1, radio signals emitted by the UAV can propagate through free space or urban environments, where they are subject to shadowing and scattering from buildings and natural obstacles, which introduce additional losses in the A2G communication link. Consequently, a G-UE experiences both small-scale fading and large-scale pathloss, each occurring with a certain probability. Assuming the UAV transmits at a power P_t, and considering a noise power σ_n^2 within the signal bandwidth, the instantaneous SNR between the G-UE and the UAV can be expressed as

$$\text{SNR} = \frac{P_t \left(\frac{\Lambda}{4\pi}\right)^2}{\sigma_n^2 l^{\alpha}} \Omega \tag{4}$$

where Λ represents the signal wavelength corresponding to the center frequency of the band, while α denotes the pathloss exponent, which is set to 2 for a Friis free-space propagation environment. The slant distance between the UAV and the G-UE is denoted by l, and is calculated as $l = \sqrt{r^2 + (h_1 - h_2)^2}$, and $\Omega \in [0, \infty]$ represents the channel power loss/gain factor, which accounts for variations in the received signal power. The model

Authorized licensed use limited to: University of the West of England. Downloaded on March 02,2025 at 08:56:53 UTC from IEEE Xplore. Restrictions apply.

This article has been accepted for inclusion in a future issue of this journal. Content is final as presented, with the exception of pagination.

for Ω is highly influenced by the ratio of signal power in the dominant LOS component to the scattered power from NLOS components. Therefore, we apply the Rician model for links to G-UEs in the first group (receivers favoring LOS conditions) and the Rayleigh model for links to G-UEs in the second group (nodes predominantly experiencing NLOS conditions), where the multipath component is the primary factor.

C. Rice Channel Model

The Rician fading model is widely used in the literature to characterize the random power loss/gain in scenarios where the signal experiences both a strong LOS path and diffuse multipath components caused by scattering from nearby rough surfaces or buildings [32]. In this case, the distribution of Ω follows a noncentral chi-square PDF for $\omega, >, 0$, as given in [33].

$$f_{\Omega_{\text{Ri}}}(\omega) = \frac{(K+1)e^{-K}}{\overline{\Omega}} e^{\frac{-(K+1)\omega}{\overline{\Omega}}} I_0\left(2\sqrt{\frac{K(K+1)\omega}{\overline{\Omega}}}\right) \quad (5)$$

where $I_0(.)$ denotes the zero-order modified Bessel function of the first kind, while $K = \frac{P_{\text{LOS}}}{P_{\text{NLOS}}}$ represents the ratio of signal power in the dominant LOS component to the scattered power from NLOS components, commonly known as the Rician K-factor. In addition, $\overline{\Omega} = 1$ is used for normalization.

D. Rayleigh Channel Model

As in terrestrial channels, for the NLOS case, the Rayleigh fading distribution typically provides a better fit and is often used to model multipath fading with no direct LOS path [32]. Hence, the parameter Ω in (4) is distributed according to Rayleigh PDF. In this case, and for $\omega > 0$, the distribution of Ω is expressed according to [33] as

$$f_{\Omega_{\text{Ra}}}(\omega) = \frac{1}{\overline{\Omega}} \exp\left(-\frac{\omega}{\overline{\Omega}}\right). \quad (6)$$

It can be shown that for $K = 0$ in (5), the Rician model reduces to a Rayleigh fading distribution with an exclusive dominance of the multipath components.

III. Altitude Dependant Coverage

In this section, we examine the UAV's ability to maximize its coverage area based on the altitude. Our analysis is set within a hybrid environment where communication links are subject to deflection and scattering. Specifically, we focus on evaluating the probability of detecting a G-UE located at the edge of the coverage area, at a distance $r = R$, which presents the worst case. This probability, referred to as the PD, represents the likelihood that the SNR at the G-UE exceeds the minimum SNR threshold required for reliable detection of the UAV's signal.

Denoting the SNR threshold by ξ, we can write a generalized expression of PD as

$$\begin{aligned}\text{PD} &= P_{\text{LOS}}\text{PD}_{\text{Ri}} + P_{\text{NLOS}}\text{PD}_{\text{Ra}} \\ &= P_{\text{LOS}}\text{Pr}\left(\frac{P_t}{l^\alpha B}\Omega_{\text{Ri}} > \xi\right) + P_{\text{NLOS}}\text{Pr}\left(\frac{P_t}{l^\alpha B}\Omega_{\text{Ra}} > \xi\right)\end{aligned} \quad (7)$$

where PD_{Ri} is the probability of detection for the Rice channel, PD_{Ra} is the probability of detection for the Rayleigh channel, and $B = (\frac{4\pi\sigma_n}{\Lambda})^2$ is introduced to simplify the notation. The computation of PD_{Ri} is given by its complementary cumulative density function (CCDF) as

$$\text{PD}_{\text{Ri}} = \int_{\sqrt{y}}^{\infty} x\, e^{\left(-\frac{x^2+2K}{2}\right)} I_0\left(\sqrt{2K}x\right) dx \quad (8)$$

where $y = 2\xi[1+K]\frac{l^\alpha}{P_t}(\frac{4\pi\sigma_n}{\Lambda})^2$. The PD for the Rice channel can then be rewritten as [33]

$$\text{PD}_{\text{Ri}} = Q\left(\sqrt{2K}, \sqrt{2\xi[1+K]l^\alpha B/P_t}\right) \quad (9)$$

where $Q(.,.)$ is the first-order Marcum Q-function. As for the CCDF in the Rayleigh scenario, according to the same reference, it can be written as

$$\text{PD}_{\text{Ra}} = \int_{\xi}^{\infty} \frac{P_t}{l^\alpha}\left(\frac{\Lambda}{4\pi\sigma_n}\right)^2 e^{-x} dx. \quad (10)$$

After integrating (10), the PD for the Rayleigh scenario turns into

$$\text{PD}_{\text{Ra}} = \frac{P_t}{l^\alpha B} e^{-\xi}. \quad (11)$$

In a hybrid environment that considers both the Rice and Rayleigh models and substituting (9) and (11) into (7), the PD turns into

$$\begin{aligned}\text{PD} = &\frac{P_t}{l^\alpha B} e^{-\xi} + \text{e}^F \\ &\times \left(Q\left(\sqrt{2K}, \sqrt{2\xi[1+K]l^\alpha B/P_t}\right) - \frac{P_t}{l^\alpha B} e^{-\xi}\right)\end{aligned} \quad (12)$$

where $F = -\frac{\lambda}{\tan(\phi)}(\frac{\tilde{h}_{\min}+\tilde{h}_{\max}}{2})$ is introduced to simplify the notation.

Fig. 2 illustrates the PD in (12), demonstrating an initial increase with altitude, followed by a decline as altitude continues to rise. This behavior is attributed to the increase of altitude h_1 that enhances the elevation angle, thereby mitigating the destructive effects of multipath scattering. However, further increasing h_1 also extends the link length, which amplifies pathloss. At lower altitudes, the reduction in multipath interference has a pronounced positive impact, leading to a sharp increase in detection probability. Conversely, at higher altitudes, the intensified path loss causes a decline in detection probability. In addition, the results indicate that the PD decreases inversely with the radius r. For a given SNR threshold ξ, as the coverage radius expands, SNR values drop, according to the model in (4), leading to poorer detection performance. However, this can be optimized by adjusting the UAV altitude based on the specific location of each ground node.

The figure reveals the presence of an optimal altitude where the effects of both multipath fading and pathloss are balanced

Authorized licensed use limited to: University of the West of England. Downloaded on March 02,2025 at 08:56:53 UTC from IEEE Xplore. Restrictions apply.

This article has been accepted for inclusion in a future issue of this journal. Content is final as presented, with the exception of pagination.

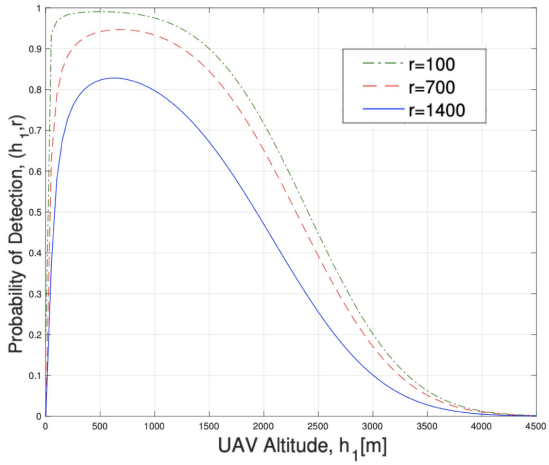

Fig. 2. PD for different coverage radii r, $\xi = 2$ dB, and $K = 5$.

for a specific radius r. Building on this, we propose investigating the influence of UAV altitude on the maximum coverage radius, constrained by a minimum SNR threshold ξ, above which the communication link is considered reliable, and for a target probability of detection $\text{PD}_{\text{target}}$. To achieve this, we compute the coverage radius R_{h_1} for a given UAV height h_1, which requires solving the following implicit equation:

$$\text{PD}(h_1, R_{\text{h}_1}) = \text{PD}_{\text{target}}. \tag{13}$$

The set of all possible pairs (h_1, R_{h_1}) presents a configuration space of the studied network among which there exist potential solutions of (13) that satisfy (7), and hence, optimize the UAV position for maximum coverage with SNR $> \xi$. To determine the optimal pair, we will use an iterative computation of (13).

IV. Altitude-Dependent SE

Next, we analyze the enhancement of the ASE, focusing on the reliable data transfer to G-UEs uniformly distributed at varying distances throughout the coverage area. The SE C is calculated based on Shannon capacity as follows:

$$C = \log_2(1 + \text{SNR}). \tag{14}$$

The SNR received by the G-UE, as expressed in (4), directly influences the SE, which depends on several key factors: the UAV's altitude, the G-UE's distance from the center, and the physical characteristics of the propagation environment, all encapsulated in the SNR model. For the Rician channel, we define the PDF of the SE, denoted as $g_{C_{\text{Ri}}}(c)$. This PDF is derived from the SNR's PDF through a random variable transformation, enabling us to capture how these parameters impact SE under the Rician fading conditions.

$$g_{C_{\text{Ri}}}(c) = 2^c \ln(2) l^\alpha \frac{B}{P_t} f_C\left((2^c - 1) l^\alpha \frac{B}{P_t}\right),\ c > 0. \tag{15}$$

Similarly, for the Rayleigh channel model, the PDF $g_{C\text{Ra}}(c)$ is deduced from the PDF of the SNR as follows:

$$g_{C_{\text{Ra}}}(c) = \frac{2^c \ln(2)}{A} e^{\left(-\frac{2^c - 1}{A}\right)},\ c > 0 \tag{16}$$

where $A = \frac{P_t}{l^\alpha B}$ is used to simplify the calculation. The A2G link between the UAV and one G-UE is considered reliable if the ASE is higher than a preset threshold C_0 determined by the desired QoS. This can be evaluated using the PC, which we define as the probability that the SE (14) be greater than the threshold C_0, expressed as

$$\begin{aligned}\text{PC} &= P_{\text{LOS}}\text{PC}_{\text{Ri}} + P_{\text{NLOS}}\text{PC}_{\text{Ra}} \\ &= P_{\text{LOS}}\text{Pr}\left(\log_2\left(1 + A\Omega_{\text{Ri}}\right) > C_0\right) \\ &\quad + P_{\text{NLOS}}\text{Pr}\left(\log_2\left(1 + A\Omega_{\text{Ra}}\right) > C_0\right).\end{aligned} \tag{17}$$

For the Rice channel model, by replacing (15) in (17) and applying a variable substitution, we obtain

$$\text{PC}_{\text{Ri}} = \int_{\sqrt{y}}^{\infty} x\, e^{\left(-\frac{x^2 + 2K}{2}\right)} I_0\left(\sqrt{2K}x\right) dx \tag{18}$$

where $y = 2[1 + K][2^{C_0} - 1]/A$. PC can be rewritten using the first-order Marcum function as

$$\text{PC}_{\text{Ri}} = Q\left(\sqrt{2K}, \sqrt{2[1 + K][2^{C_0} - 1]/A}\right). \tag{19}$$

Also, in the case of the Rayleigh channel model, we can express the PC as

$$\text{PC}_{\text{Ra}} = \int_{C_0}^{\infty} \frac{2^c \ln(2)}{A} e^{\left(-\frac{2^c - 1}{A}\right)} dc. \tag{20}$$

To facilitate the calculation, we do a variable substitution in (20) where $c = \log(x)$, which means $x = 2^c$. Hence, the expression of the probability turns into

$$\text{PC}_{\text{Ra}} = e^{\left(-\frac{\ln(C_0) - 1}{A}\right)}. \tag{21}$$

When examining the hybrid environment of both the Rice and Rayleigh models, the final expression of the PC becomes

$$\begin{aligned}\text{PC} = e^{-\frac{\ln(C_0) - 1}{A}} + e^F \times \\ \left(Q\left(\sqrt{2K}, \sqrt{2[1 + K][2^{C_0} - 1] l^\alpha B/P_t}\right) - e^{-\frac{\ln(C_0) - 1}{A}}\right).\end{aligned} \tag{22}$$

The results in Fig. 3 show that the PC exhibits the same behavior as the PD, which is expected due to the relationship in (14). While the PC provides a slightly larger coverage radius for a given height, its maximum is slightly lower. This means that the PC can also be maximized for a given altitude h_1 and a coverage radius r.

The objective is to determine the optimal altitude h_1 for the UAV to maximize the connectivity area while achieving a target probability of coverage $\text{PC}_{\text{target}}$ that ensures a minimum ASE of C_0. Our focus is on optimizing the ASE for all G-UEs within the coverage boundary. These G-UEs are uniformly distributed at varying distances from the center, O. The ASE, represented as $\bar{C}$, is computed by averaging the capacity C, as given in (14), across the coverage area with radius R, taking into account the different distances r of the G-UEs. The optimal altitude h_1 for the averaged rate can then be found by numerically solving the

Authorized licensed use limited to: University of the West of England. Downloaded on March 02,2025 at 08:56:53 UTC from IEEE Xplore. Restrictions apply.

This article has been accepted for inclusion in a future issue of this journal. Content is final as presented, with the exception of pagination.

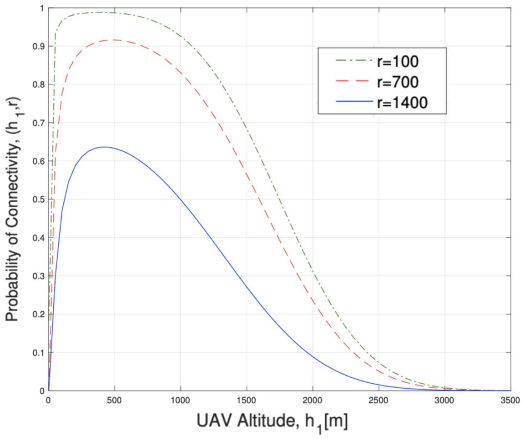

Fig. 3. PC for different coverage radius r, $C_0 = 2$, and $K = 5$.

following equation:

$$\mathrm{PC}(h_1, R_{\mathrm{h}_1}) = \mathrm{PC}_{\mathrm{target}}. \tag{23}$$

The set of all possible pairs (h_1, R_{h_1}) here stands for the potential solutions satisfying (17) for an ASE $\bar{C} > C_0$.

V. Rician *K*-Factor Models

The *K*-factor is defined as the ratio of the signal power in the dominant component to the local-mean scattered power. Since the prominence of the LOS component can vary across different locations, ground nodes may experience varying Rician factor models even when communicating with the same UAV. In this context, we explore the influence of the *K*-factor model on the network performance from two additional perspectives.

A. K-Factor in a Rough Surface

In this case, the value of *K* changes depending on the horizontal displacement of the UAV relative to the ground node for a UAV at a certain height. So, the *K*-factor can be expressed with the normalization as [34]

$$K = \frac{1}{<|\rho^2|>} \tag{24}$$

where $<|\rho^2|>$ is the mean square power from the scattered components and is expressed as

$$<|\rho^2|> = \int_{h_2\cot 2\beta_0}^{h_1\cot 2\beta_0} \frac{l^2\cot^2\beta_0}{(\pi(h_2^2+x^2)(h_1^2+(r-x)^2)\cos^4\beta)} \times \exp\left(-\frac{\tan^2\beta}{\tan^2\beta_0}\right) dx \tag{25}$$

where β is the angle formed by the bisector of the incident and dispersed rays with the z-axis, and β_0 is the area contributing to the diffused component of the reflected ray, given by

$$\tan(\beta_0) = \frac{2\sigma}{T} \tag{26}$$

for σ the standard deviation of normally distributed height variations, and T is the horizontal auto-correlation distance.

Fig. 4 illustrates the behavior of PD and PC as functions of UAV altitude across both suburban and urban environments,

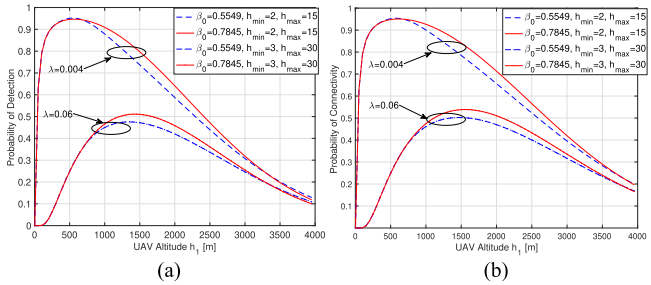

Fig. 4. PD and PC for the physics-based Rician *K*-factor model for $r = 700$ m. (a) $\xi = 1$ dB, $\mathrm{PD}_{\mathrm{target}} = 0.9$. (b) $C_0 = 1$, $PC_{\mathrm{target}} = 0.9$.

considering two distinct soil roughness values. As expected from the relationship in (14), PC and PD follow a similar trend: they increase with altitude until reaching a peak, after which they decline as the altitude continues to rise. This is due to the fact that as the altitude h_1 increases, the link length grows, leading to higher pathloss. At lower altitudes (below 500 m in suburban areas and below 1000 m in urban environments), the impact of ground roughness on the probabilities is negligible, and both values of β_0 yield similar performance. This results from the high SNR, which ensures reliable detection for the target probability of 0.9. However, at higher altitudes, greater ground roughness (higher β_0 values) becomes beneficial for communication, as the scattered signal components are more easily detected at larger elevation angles.

B. K-Factor in a Concrete Surface

In this case, the dependence of *K* on different values of height h_1 and distance r is determined by their ratio. We are going to consider a general relationship between *K* and ϕ characterized by the following relation:

$$K = ae^{b\phi} \quad \text{for} \quad \phi \in [0, \pi/2] \tag{27}$$

where a and b are constants depending on the environment and on the system parameters. Such dependence is supported by the empirical data presented in [35]. The constants a and b can be determined as

$$a = \kappa_0, \quad b = \frac{2}{\pi}\ln\left(\frac{\kappa_{\frac{\pi}{2}}}{\kappa_0}\right) \tag{28}$$

where κ_0 and $\kappa_{\frac{\pi}{2}}$ are as defined in [23, Lemma 2] and could be determined from measurements on a concrete surface.

Fig. 5 illustrates PD and PC in both urban and suburban environments, considering various ground parameters. Similar to the case of rough soil, a comparable behavior is observed; however, the peak probabilities are notably higher, approaching nearly 1 in suburban area and around 0.7 in urban one. In contrast to the curves in Fig. 4, which begin to decline at lower altitudes, the curves in this figure maintain elevated probabilities even at significantly higher altitudes up to 2500 m for PD and 3000 m for PC. This underscores the sensitivity of the rough surface model to pathloss variations. In addition, the material characteristics of concrete, particularly $\kappa_{\pi/2}$ and κ_0, influence the probabilities, especially at altitudes exceeding 1500 m. Higher values of $\kappa_{\pi/2}$ correspond to larger K values,

Authorized licensed use limited to: University of the West of England. Downloaded on March 02,2025 at 08:56:53 UTC from IEEE Xplore. Restrictions apply.

This article has been accepted for inclusion in a future issue of this journal. Content is final as presented, with the exception of pagination.

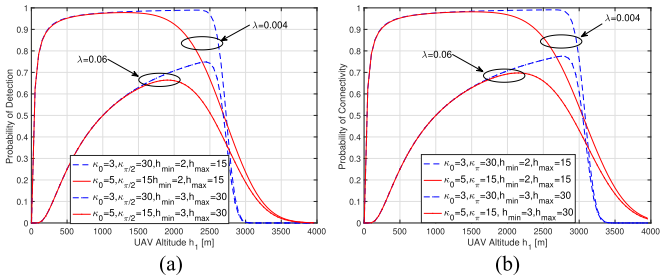

Fig. 5. PD and PC for the exponential Rician K-factor model, $r = 700$ m. (a) $\xi = 1$ dB, $\text{PD}_{\text{target}} = 0.9$. (b) $C_0 = 1$, $\text{PC}_{\text{target}} = 0.9$.

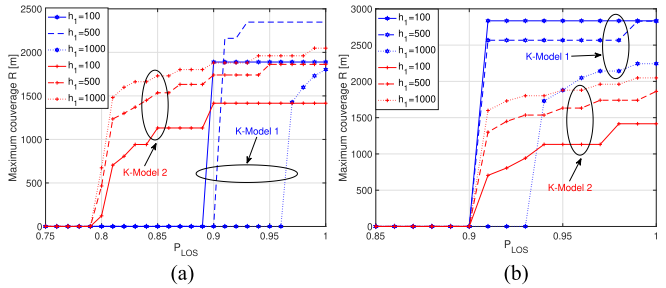

Fig. 6. PD and PC as functions of P_{LOS}, (a) $\xi = 1$ dB, $\text{PD}_{\text{target}} = 0.9$. (b) $C_0 = 1$, $\text{PC}_{\text{target}} = 0.9$.

signifying a stronger LOS component, which in turn results in a greater peak probability compared to lower $\kappa_{\pi/2}$ values.

VI. Optimal Altitude Search Analysis

In this section, we analyze the dependence between different parameters and the performance of the considered network scenario, where a UAV is placed to maximize the coverage radius subject to signal strength and SE. In the considered model, link assessment can be achieved at the level of ground nodes, yet the interaction of link state information required to assist the UAV in selecting the optimal position leads to an extra overhead and communication delay. Hence, we assume the optimization process to be performed at the level of the UAV. The analysis is carried out in urban and suburban environments with a probabilistic LOS model as described in Section II-A. The Rayleigh model is used to characterize the NLOS profile, while the Rice model is used to characterize the LOS profile. In both the urban and suburban environments, we compare the results for the two K-factor models corresponding to the rough surface and concrete surface that we denote as K-model 1 and K-model 2, respectively. We recall that K-model 2 was initially used in [23] for the case of the LOS channel with free-space transmission.

A. Dependence of P_{LOS}, R, and h_1

The maximum coverage radius R obtained for detection/connection probability target 0.9 is presented in Fig. 6 for the two considered K-factor models and different UAV altitudes. In Fig. 6(a), it is evident that PD increases as a function of P_{LOS} across all configurations, with a notable rise in altitude for K-model 2, while for K-model 1, PD decreases

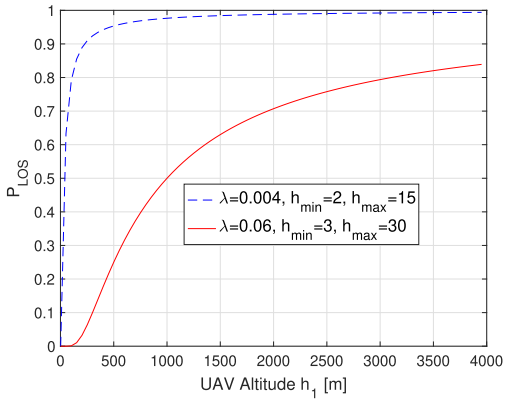

Fig. 7. P_{LOS} in suburban (blue) and urban (red) environments.

with altitude. At low altitudes ($h_1 = 100$ m), the maximum coverage radius reaches 1900 m for K-model 1 and 1400 m for K-model 2, although this requires a significant P_{LOS} (>0.9). For higher altitudes, K-model 2 provides broader coverage, even with lower P_{LOS} values, such as >0.83 at $h_1 = 500$ m and >0.81 at $h_1 = 1000$ m. This behavior reverses with K-model 1, where the maximum coverage reaches 2400 m for $h_1 = 500$ m, then declines to 1700 m at $h_1 = 1000$ m. This reduction is attributed to the increased attenuation from the rough ground, which scatters signals and ultimately diminishes the overall SNR.

When using the channel capacity as a metric for measuring connectivity, Fig. 6(b) demonstrates that the maximum coverage radius expands, allowing devices to transmit and receive data over longer distances, even with lower SNR values. However, a strong LOS component ($P_{\text{LOS}} > 0.9$) is necessary across all system configurations. Similar to the previous case, in K-model 2, coverage increases steadily as h_1 rises. Conversely, in K-model 1, the coverage radius is larger at lower h_1 values, and it is possible to cover the same area at higher altitudes when the LOS component is stronger. Overall, it is observed that in rough ground conditions (K-model 1), wider coverage can be achieved at lower altitudes compared to concrete ground conditions (K-model 2), which helps conserve energy by reducing the need to position the UAV at higher altitudes.

Fig. 7 illustrates the LOS probability as a function of UAV altitude in two distinct propagation environments: 1) suburban, with parameters $\lambda = 0.004$, $h_{\text{min}} = 2$ m, and $h_{\text{max}} = 15$ m, and 2) urban, with $\lambda = 0.06$, $h_{\text{min}} = 3$ m, and $h_{\text{max}} = 30$ m. These values were experimentally determined in [31]. In both environments, P_{LOS} increases steadily as the UAV altitude rises for a fixed radius R, eventually plateauing at approximately 500 m in suburban area and around 3000 m in urban area. This behavior is expected since P_{LOS} is an exponential function of the elevation angle ϕ, which is directly proportional to the altitude. In addition, as building density (λ) increases, P_{LOS} decreases correspondingly.

B. Simulation Setup

The results reported in this section are based on the probability of PD and the PC. The two probabilities are evaluated numerically to assess the largest radius satisfying a reliable connection

Authorized licensed use limited to: University of the West of England. Downloaded on March 02,2025 at 08:56:53 UTC from IEEE Xplore. Restrictions apply.

This article has been accepted for inclusion in a future issue of this journal. Content is final as presented, with the exception of pagination.

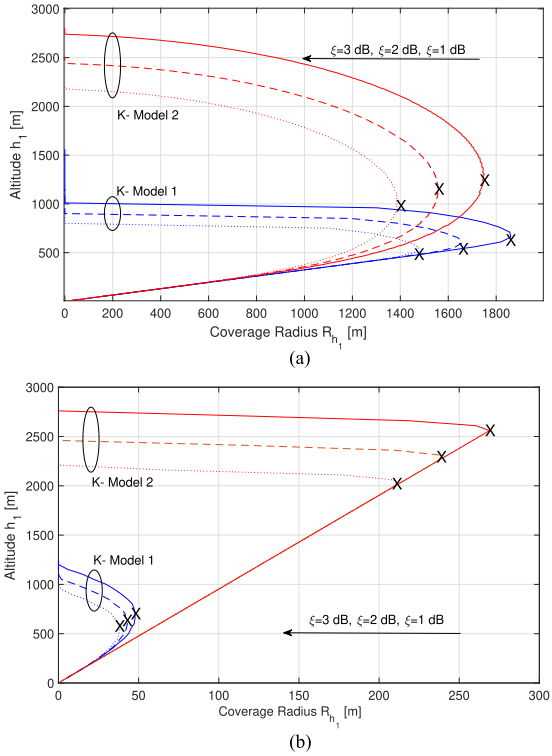

Fig. 8. Set of configuration space of pairs (h_1, R_{h_1}) for $\text{PD}_{\text{target}} = 0.9$ and different values of SNR threshold ξ in urban and suburban environments.

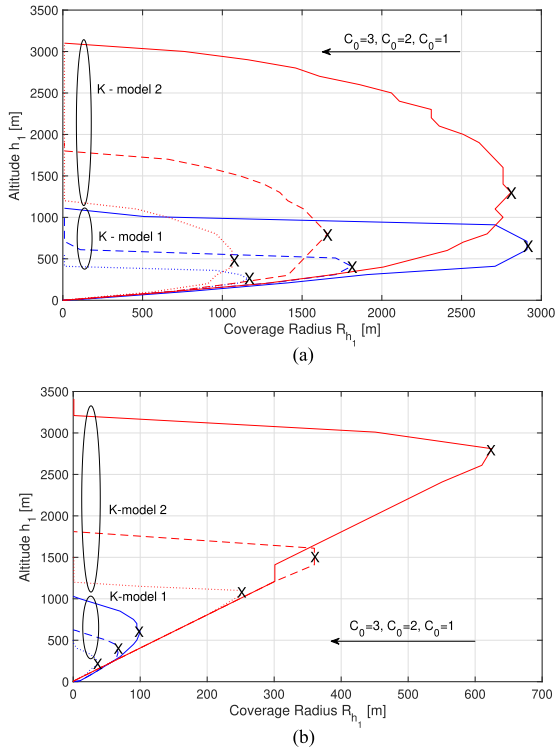

Fig. 9. Set of configuration space of pairs (h_1, R_{h_1}) for $\text{PC}_{\text{target}} = 0.9$ and different values of SE C_0 in urban and suburban environments.

with a target of 0.9 for different threshold values of SNR $\xi > 0$ and SE $C_0 > 0$. The maximum heights of the buildings are equal to $h_{\max} \in \{15\text{ m}, 30\text{ m}\}$, the minimum height of buildings is $h_{\min}$ =2 m, the elevation angle ϕ is in $\{0, \pi/2\}$, and the parameter λ of the Poisson process is equal to 0.004 and 0.06, respectively for the case of suburban and urban environments. These parameters are derived from the study presented in [31]. For the different *K*-factor models, we use the same parameters as in Section V, particularly, $\beta_0 = 0.5549$ in *K*-model 1, which corresponds to the rough surface, and the parameters $\kappa_0 = 3$ and $\kappa_{\frac{\pi}{2}} = 30$ in *K*-model 2 that corresponds to the concrete surface. It is assumed that $B/P_t = 70$ dB and the ASE $\bar{C}$ is obtained over 200 uniformly distributed G-UEs.

C. Results and Discussions

Fig. 8 illustrates the set of all pairs (h_1, R_{h_1}) that satisfy the condition in (13) for *K*-model 1 (blue curves) and *K*-model 2 (red curves), across three different SNR threshold values in both suburban and urban environments. In all configurations and for both *K*-models, a unique optimal height h_1 emerges, maximizing the coverage radius R. As expected, for each altitude h_1, the coverage radius R_{h_1} decreases as the SNR threshold ξ increases, although the decline is more pronounced at higher altitudes. The locations of the optimal solutions $(h_{1,\text{opt}}, R_{h_{1,\text{opt}}})$, marked with "$\times$" on the figure, reveal an interesting observation: the elevation angle ϕ remains constant across all SNR threshold values, indicating that ϕ is independent of the SNR threshold. However, the value of the optimal altitude $h_{1,\text{opt}}$ decreases as ξ increases. This behavior can be explained by the fact that higher SNR thresholds degrade the PD, resulting in a reduced coverage radius R for the same target probability of detection $\text{PD}_{\text{target}}$.

We also observe that building density and height in urban environments severely restrict the coverage radius, reducing it from approximately 1800 m in suburban settings to less than 50 m for *K*-model 1 and 300 m for *K*-model 2 in urban areas. This outcome intuitively reflects the negative impact of the absence of LOS components on PD, due to high building density along the line connecting the UAV and ground nodes (with a building density of $\lambda = 0.06$). Figs. 4 and 5 illustrate this limitation, showing that the maximum coverage radius does not exceed 0.5 and 0.7 for *K*-model 1 and *K*-model 2, respectively, when $r = 700$ m. In Figs. 4(a) and 5(a), it is evident that the target detection probability is only achieved within a very limited area, with *K*-model 2 offering a slightly larger radius, highlighting the performance constraints imposed by rough surfaces when LOS components are absent. In line with the results depicted in Figs. 6 and 7, for altitudes below 1000 m, the LOS probability (P_{LOS}) remains below 0.5, favoring NLOS components, which are disadvantageous for the scenarios under study. To ensure the required QoS with a target detection probability of $\text{PD}_{\text{target}} = 0.9$, P_{LOS} must exceed 0.8 for *K*-model 1 and 0.89 for *K*-model 2.

Fig. 9 illustrates the set of all configuration pairs (h_1, R_{h_1}) that satisfy the constraint in (23) for both urban and suburban environments. Similarly to the previous results, the variation in system parameters impacts both PD and the PC in a consistent manner. Notably, increasing the SE threshold C_0 significantly reduces the probability of reliable connectivity in both models.

Authorized licensed use limited to: University of the West of England. Downloaded on March 02,2025 at 08:56:53 UTC from IEEE Xplore. Restrictions apply.

This article has been accepted for inclusion in a future issue of this journal. Content is final as presented, with the exception of pagination.

In addition, decreasing the Poisson parameter $\lambda = 0.004$, which represents the number of buildings per square kilometer along the distance between the UAV and the ground users, as well as lowering the maximum building height $h_{\max}$, leads to higher values of both PC and PD. For *K*-model 2, however, achieving the same coverage radius with the required SE demands higher altitudes compared to *K*-model 1. In urban environments, the coverage radius offering the required SE for *K*-model 2 is notably limited, and further increases in altitude fail to improve SE at larger radii. Instead, the coverage diminishes to 0 m at very high altitudes due to severe pathloss caused by the extended distance l.

Examining the behavior of the curves, we again observe two distinct regimes, with a unique optimal altitude $h_{1,\text{opt}}$ emerging for all possible system configurations. This optimal altitude maximizes the coverage radius $R_{h_1,\text{opt}}$, ensuring that the required ASE ($\bar{C} > C_0$) is met for ground UEs located within the coverage area. However, consistently with the findings in Fig. 6, a significantly larger connectivity radius is achieved when using the SE in (14) as a metric, rather than the signal strength in (4). Notably, the maximum connectivity radius surpasses 2600 m in suburban environments and 200 m in urban settings, nearly doubling the previously recorded values. In addition, the optimal altitudes required to guarantee the SE decrease as the SE threshold C_0 decreases. Examining the optimal pairs ($h_{1,\text{opt}}$, $R_{h_1,\text{opt}}$), we note that optimizing for each SE threshold C_0 results in a constant elevation angle ϕ, which remains unaffected by the values of C_0.

The results demonstrate that across all system configurations, as the altitude h_1 increases, the corresponding coverage radius R_{h_1} initially expands, reaching a maximum value before eventually narrowing. This indicates that at lower altitudes, the reduction in multipath effects, achieved by increasing height, is beneficial for coverage. However, beyond a certain point, further altitude increases lead to diminishing returns, as pathloss becomes the dominant factor, reducing the coverage radius. Between these two regimes, the curves reveal a unique optimal altitude, corresponding to the same elevation angle ϕ_{opt}, which represents the optimal configuration ($h_{1,\text{opt}}$, $R_{h_1,\text{opt}}$) for ensuring the required reliability. At the optimal configuration, it is possible to further enhance the coverage through increasing the transmission power. Importantly, this optimal angle ϕ_{opt} remains invariant across all SNR or SE threshold values, highlighting its independence from these thresholds. This observation holds true for both Rician *K*-factor models and in both suburban and urban environments.

The optimal position provides the largest coverage; however, it is important to emphasize that link reliability is maintained across the entire set of solutions (h_1, R_{h_1}) shown in Figs. 8 and 9. Notably, for each coverage radius R, there are two altitude values that guarantee the desired QoS. For example, if the target coverage radius is $R = 800$ m and the SNR threshold is $\xi = 2$ dB, the UAV can be positioned at either $h_1 = 250$ m or $h_1 = 1000$ m for *K*-model 1, and at $h_1 = 250$ m or $h_1 = 2250$ m for *K*-model 2. Moreover, under the same environmental and system conditions, the optimal coverage radius $R_{h_1,\text{opt}} = 1650$ m can be achieved by placing the UAV at an altitude of $h_{1,\text{opt}} = 500$ m for *K*-model 1, or $h_{1,\text{opt}} = 1100$ m for *K*-model 2. These flexible altitude options make the solution highly adaptable to real-world scenarios involving low-altitude platforms, allowing for practical implementation across various operational conditions.

In urban environments, where the P_{LOS} is low, flying above concrete surfaces proves to be significantly more advantageous than over rough surfaces, offering up to five times greater coverage. In contrast, in suburban areas, where P_{LOS} is generally higher, both surface types deliver comparable performance in terms of coverage radius. In addition, in both urban and suburban settings, the UAV must be positioned at a considerably higher altitude, at least double, when flying over concrete surfaces compared to rough ones in order to maintain equivalent performance. This is primarily due to the need to mitigate the negative impact of multipath scattering, which is more pronounced near concrete surfaces.

VII. Conclusion

This article explores UAV-assisted ground wireless network configurations to ensure reliable connections. The study focuses on a hybrid environment that utilizes a probabilistic LOS model, accounting for the effects of varying multipath fading patterns based on the UAV's altitude and elevation angle. We conducted an in-depth analysis of how network performance, specifically coverage and connectivity, depends on UAV altitude and LOS probability. Our findings indicate that there is an optimal altitude for positioning the UAV that maximizes the deployment area of ground nodes. Interestingly, this optimal position occurs at the same elevation angle across all metrics considered.

Moreover, our investigation into the impact of LOS probability reveals that LOS components are critical for the successful deployment of UAV-assisted networks. In urban environments, coverage is five times lower than in suburban areas when the UAV operates over concrete surfaces with strong LOS components. This disparity becomes even more pronounced up to 30 times lower when the UAV flies over rough soil, which has weaker LOS components. These results emphasize the profound influence of the physical properties of the ground on network performance.

This study investigates coverage enhancement through altitude optimization across various scenarios. Building on this foundation, our ongoing work delves into the impact of interference, focusing on the performance of communication systems in swarm-based configurations. By optimizing UAV density and accounting for higher ground user density, we aim to maximize network coverage while minimizing interference from other aerial components and ground infrastructure. In addition, future research will explore other critical influencing factors, such as adverse weather conditions. Specifically, phenomena such as strong winds and heavy rainfall, which can destabilize UAVs and hinder their ability to maintain steady positions or flight paths, will be thoroughly analyzed.

References

[1] P. Popovski, K. F. Trillingsgaard, O. Simeone, and G. Durisi, "5G wireless network slicing for eMBB, URLLC, and mMTC: A communication-theoretic view," *IEEE Access*, vol. 6, pp. 55765–55779, 2018.

Authorized licensed use limited to: University of the West of England. Downloaded on March 02,2025 at 08:56:53 UTC from IEEE Xplore. Restrictions apply.

This article has been accepted for inclusion in a future issue of this journal. Content is final as presented, with the exception of pagination.

[2] L. Nasraoui, A. Dabbar, and M. Siala, "Energy and MCS optimization in HARQ protocol for ultrareliable regime with maximized throughput," *IEEE Syst. J.*, vol. 17, no. 1, pp. 1282–1291, Mar. 2023.
[3] Y. Hwang and S. Oh, "A study on ultra-reliable and low-latency communication technologies for 5G & 6G services," in *Proc. 13th Int. Conf. Inf. Commun. Technol. Convergence*, Oct. 2022, pp. 1207–1209.
[4] L. Nasraoui, L. N. Atallah, and M. Siala, "Performance analysis of low-complexity simply-differential time synchronization approach for MTC over LTE systems," in *Proc. IEEE 84th Veh. Technol. Conf.*, Sep. 2016, pp. 1–5.
[5] L. Nasraoui, "Partial contention-free D2D discovery for proximity-based services in cellular networks," in *Proc. Int. Conf. Smart Commun. Netw. Technol.*, Oct. 2018, pp. 177–182.
[6] Q. Wu et al., "A comprehensive overview on 5G-and-beyond networks with UAVs: From communications to sensing and intelligence," *IEEE J. Sel. Areas Commun.*, vol. 39, no. 10, pp. 2912–2945, Oct. 2021.
[7] A. N. Wilson, A. Kumar, A. Jha, and L. R. Cenkeramaddi, "Embedded sensors, communication technologies, computing platforms and machine learning for UAVs: A review," *IEEE Sensors J.*, vol. 22, no. 3, pp. 1807–1826, Feb. 2022.
[8] L. Nasraoui and S. Ikki, "Robust D2D neighbor discovery through SideLink demodulation reference signal for LTE network," in *Proc. IEEE 30th Annu. Int. Sym. Pers., Indoor Mobile Radio Commun.*, Sep. 2019, pp. 1–5.
[9] L. Nasraoui and S. Ikki, "Neighbor discovery for ProSe and V2X communications," *IEEE Internet Things J.*, vol. 8, no. 9, pp. 7241–7251, May 2021.
[10] K. V. Katsaros et al., "Connected and automated mobility services in 5G cross-border environments: Challenges and prospects," *IEEE Intell. Transp. Syst. Mag.*, vol. 15, no. 3, pp. 145–157, May/Jun. 2023.
[11] R. Casellas, R. Vilalta, R. Martinez, and R. Munoz, "Highly available SDN control of flexi-grid networks with network function virtualization-enabled replication," *IEEE/OSA J. Opt. Commun. Netw.*, vol. 9, no. 2, pp. A207–A215, Feb. 2017.
[12] A. I. Hentati and L. C. Fourati, "Mobile target tracking mechanisms using unmanned aerial vehicle: Investigations and future directions," *IEEE Syst. J.*, vol. 14, no. 2, pp. 2969–2979, Jun. 2020.
[13] L. Nasraoui and L. Najjar, "SRS-Based D2D neighbor discovery scheme for LTE cellular networks," in *Proc. IEEE 28th Annu. Int. Symp. Pers., Indoor Mobile Radio Commun.*, Oct. 2017, pp. 1–5.
[14] J. Tang et al., "BTV-CMAB: A bi-directional trust verification-based combinatorial multiarmed bandit scheme for mobile crowdsourcing," *IEEE Internet Things J.*, vol. 11, no. 2, pp 1925–1938, Jan. 2024.
[15] Y. Ren, W. Liu, A. Liu, T. Wang, and A. Li, "A privacy-protected intelligent crowdsourcing application of IoT based on the reinforcement learning," *Future Gener. Comput. Syst.*, vol. 127, pp 56–69, Feb. 2022.
[16] M. A. Khan et al., "Swarm of UAVs for network management in 6 G: A technical review," *IEEE Trans. Netw. Serv. Manage.*, vol. 20, no. 1, pp. 741–761, Mar. 2023.
[17] B. Zarai, L. Nasraoui, R. Bousaada, and S. Boudjit, "6G-enabled situation-aware ML-assisted UTM (6G-SAMU)," in *Proc. Int. Wireless Commun. Mobile Comput. Conf.*, May 2024, pp. 1797–1802.
[18] R. Shrestha, R. Bajracharya, and S. Kim, "6 G enabled unmanned aerial vehicle traffic management: A perspective," *IEEE Access*, vol. 9, pp. 91119–91136, 2021.
[19] J. Primicerio, A. Matese, S. D. Gennaro, L. Albanese, S. Guidoni, and P. Gay, "Development of an integrated, low-cost and opensource system for precision viticulture: From UAV to WSN," in *Proc. EFITA-WCCA-CIGR Conf. Sustain. Agriculture Through ICT Innov.*, Jun. 2013, pp. 23–27.
[20] T. Kunz and B. Tatham, "Localization in wireless sensor networks and anchor placement," *J. Sens. Actuator Netw.*, vol. 1, pp. 36–58, Apr. 2012.
[21] A. Sellami, L. Nasraoui, and L. Najjar, "Neighbor-assisted localization for massive MIMO 5G systems," in *Proc. Int. Multi-Conf. Syst., Signals Devices*, Mar. 2021, pp. 503–509.
[22] A. Sellami, L. Nasraoui, and L. Najjar, "Outdoor neighbor-assisted localization algorithm for massive MIMO systems," in *Proc. IEEE 94th Veh. Technol. Conf.*, Mar. 2021, pp. 1–5.
[23] M. M. Azari, F. Rosas, K-C. Chen, and S. Pollin, "Ultra reliable UAV communication using altitude and cooperation diversity," *IEEE Trans. Commun.*, vol. 33, no. 1, pp. 330–344, Jan. 2018.
[24] L. Nasraoui and S. Roy, "Optimal UAV positioning for terrestrial user," in *Proc. IEEE 91st Veh. Technol. Conf.*, May 2020, pp. 1–5.
[25] T. Sivalingam, K. B. S. Manosha, N. Rajatheva, M. Latva-aho, and M. B. Dissanayake, "Positioning of multiple unmanned aerial vehicle base stations in future wireless network," in *Proc. IEEE 91st Veh. Technol. Conf.*, May 2020, pp. 1–6.
[26] Z. Dai, Y. Zhang, W. Zhang, X. Luo, and Z. He, "A multi-agent collaborative environment learning method for UAV deployment and resource allocation," *IEEE Trans. Signal Inf. Process. Over Netw.*, vol. 8, pp. 120–130, 2022.
[27] Z. Wang et al., "Toward reliable UAV-enabled positioning in mountainous environments: System design and preliminary results," *IEEE Trans. Rel.*, vol. 71, no. 4, pp. 1435–1463, Dec. 2022.
[28] M. J. Sobouti et al., "Efficient fuzzy-based 3-D flying base station positioning and trajectory for emergency management in 5G and beyond cellular networks," *IEEE Syst. J.*, vol. 18, no. 2, pp. 814–825, Jun. 2024.
[29] 3GPP, "Enhanced LTE support for aerial vehicles," 3GPP TR 36.777 Nov. 2019. [Online]. Available: ftp://www.3gpp.org/specs/archive/36_series/36.777
[30] P. Kyosti et al., "WINNER II channel models," WINNER II Public Deliverable D1.1.2 V1.0, Sep. 2007.
[31] S. Roy and M. Mehrnoush, "A new Poisson process based model for LOS/NLOS discrimination in clutter modeling," *IEEE Trans. Antennas Propag.*, vol. 67, no. 12, pp. 7538–7549, Dec. 2019.
[32] D. W. Matolak, "Air-ground channels & models: Comprehensive review and considerations for unmanned aircraft systems," in *Proc. IEEE Aerosp. Conf.*, Mar. 2012, pp. 1–17.
[33] M. K. Simon and M-S. Alouini, *Digital Communication Over Fading Channels*. Hoboken, NJ, USA: Wiley, 2000.
[34] A. Spizzichino and P. Beckmann, *Scattering of Electromagnetic Waves From Rough Surfaces*, (International series of monographs on Electromagnetic Waves). New York, NY, USA: MacMillan, 1963.
[35] Iskandar and S. Shimamoto, "Channel characterization and performance evaluation of mobile communication employing stratospheric platforms," in *Proc. IEEE/ACES Int. Conf. Wireless Commun. Appl. Comput. Electromag.*, Apr. 2005, pp. 828–831.

Bilel Ben Saoud (Student Member, IEEE) received the engineering degree in computer science from the National School of Engineering of Carthage (ENICAR), Carthage, Tunisia, in 2020, and the master's degree in computer sciences (specialized in Internet of Things) from the National School of Computer Sciences (ENSI), University of Manouba, Manouba, Tunisia, in 2021.

His research interests include the performance optimization of unmanned-aerial-vehicle-assisted networks.

Leïla Nasraoui (Senior Member, IEEE) received the M.S. degree in telecommunications and the Ph.D. degree in information and communication technologies from the Higher School of Communications (SUP'COM), University of Carthage, Carthage, Tunisia, in 2010 and 2015, respectively.

She is currently an Associate Professor of telecommunications with the National School of Computer Sciences (ENSI), University of Manouba, Manouba, Tunisia. She was also an International Professional Visiting Scholar with the Department of Electrical and Computer Engineering, University of Washington, Seattle, WA, USA. Her research interests include emerging network design and optimization with special emphasis on proximity services and public safety communications, Internet of Things, unmanned aerial vehicle communication, and vehicular networks.

Dr. Nasraoui was the recipient of various awards including L'Oréal-UNESCO For Women in Science in 2019 and Pierre Simon de Laplace in 2024, and was selected for the Fulbright Visiting Scholar Program for 2024–2025. She served as a Technical Program Committee member for various conferences, including 2018 IEEE International Symposium on Personal, Indoor and Mobile Radio Communications (PIMRC), IEEE International Conference on High Performance Switching and Routing in 2021, 2022, and 2025, Joint European Conference on Networks and Communications and 6G Summit 2021 and 2022, IFIP/IEEE International Conference on Performance Evaluation and Modeling in Wired and Wireless Networks in 2023 and 2024, and 2025 IEEE Wireless Communications and Networking Conference, and has reviewed journal and conferences papers, such as IEEE TRANSACTIONS ON VEHICULAR TECHNOLOGY, IEEE SIGNAL PROCESSING LETTERS, IEEE SYSTEMS JOURNAL, IEEE TRANSACTIONS ON INDUSTRIAL INFORMATICS, 2021 IEEE International Conference on Communications, IEEE ACCESS, IEEE Global Communications Conference, IEEE PIMRC, etc.

Authorized licensed use limited to: University of the West of England. Downloaded on March 02,2025 at 08:56:53 UTC from IEEE Xplore. Restrictions apply.